


REVIEW ARTICLE

Projected increase of the East Asian summer monsoon (*Meiyu*) in Taiwan by climate models with variable performance

Yu-Shiang Tung¹  | S.-Y. Simon Wang² | Jung-Lien Chu¹ | Chi-Hua Wu³ | Yung-Ming Chen¹ | Chao-Tzuen Cheng¹ | Lee-Yaw Lin¹

¹National Science and Technology Center for Disaster Reduction, Taipei, Taiwan

²Department of Plants, Soils and Climate, Utah State University, Logan, UT

³Research Center for Environmental Changes, Academia Sinica, Taipei, Taiwan

Correspondence

Shih-Yu Simon Wang, Plants, Soil and Climate Department/Utah Climate Center, Utah State University, 4825 Old Main Hill, Logan, UT 84322.
Email: simon.wang@usu.edu

Funding information

Ministry of Science and Technology, Grant/Award Number: MOST 107-2621-M865-001; Office of Science, Grant/Award Number: DE-SC0016605

Abstract

The active phase of the East Asian summer monsoon (EASM) in Taiwan during May and June, known as *Meiyu*, produces substantial precipitation for water uses in all sectors of society. Following a companion study that analysed the historical increase in the *Meiyu* precipitation, the present study conducted model evaluation and diagnosis based on the EASM lifecycle over Taiwan. Higher and lower skill groups were identified from 17 Couple Model Intercomparison Project Phase 5 (CMIP5) models, with five models in each group. Despite the difference in model performance, both groups projected a substantial increase in the *Meiyu* precipitation over Taiwan. In the higher skill group, weak circulation changes and reduced low-level convergence point to a synoptically unfavourable condition for precipitation. In the lower skill group, intensified low-level southwesterly winds associated with a deepened upper level trough enhance moisture pooling. Thus, the projected increase in *Meiyu* precipitation will likely occur through the combined effects of (1) the extension of a strengthened North Pacific anticyclone enhancing southwesterlies; and (2) more systematically, the Clausius–Clapeyron relationship that increases precipitation intensity in a warmer climate. The overall increase in the *Meiyu* precipitation projected by climate models of variable performance supports the observed tendency toward more intense rainfall in Taiwan and puts its early June 2017 extreme precipitation events into perspective.

KEYWORDS

climate change, model performance, monsoon

1 | INTRODUCTION

Located in the central region of the East Asian summer monsoon (EASM) (Figure 1a), Taiwan undergoes a pronounced precipitation sequence following the signature

lifecycle of the EASM's active–break–revival–retreat phases (Figure 1b) (Chen *et al.*, 2004; Takahashi and Yasunari, 2006). The active phase of the EASM, known as *Meiyu* in Taiwan, is characterized by a substantial increase in rainfall which produces much needed water

This is an open access article under the terms of the Creative Commons Attribution License, which permits use, distribution and reproduction in any medium, provided the original work is properly cited.

© 2020 The Authors. Meteorological Applications published by John Wiley & Sons Ltd on behalf of the Royal Meteorological Society.

for agricultural, industrial and residential uses after a prolonged dry season. The timely arrival of *Meiyu* is critical because it can mitigate a drought situation, as was the case during 2015 when the arrival of a moderate *Meiyu* ended Taiwan's worst drought in 67 years. However, extreme rainfall and flooding also come with *Meiyu*. For example, an early June 2017, a rainstorm embedded in the *Meiyu* frontal zone dumped 210 mm of rainfall over 3 hr in northern Taiwan, submerging two Taiwanese townships with US\$9 million of agriculture loss. Wang *et al.* (2016) found that *Meiyu* rainfall in Taiwan has intensified since 1990 while shifting later in the season (from late May to early June). Huang and Chen (2015) observed that Taiwan's *Meiyu* rainfall has

transitioned from a predominately frontal regime to an increasingly convective regime. Likewise, in southern China, Luo and Zhang (2015) also observed that *Meiyu* rainfall has tended to arrive later during the past two decades.

The rain band associated with *Meiyu* (Figure 1a) is initiated and sustained by instability and adiabatic ascent embedded in the mid-tropospheric warm advection and transient eddies, and these are fuelled by moisture supply from the tropical warm pool (Sampe and Xie, 2010). Figure 1a illustrates the atmospheric features of the 850 hPa winds and meridional temperature gradient overlaid with precipitation during May 20–June 10, that is, the climatological *Meiyu* period (Figure 1b). Possible future

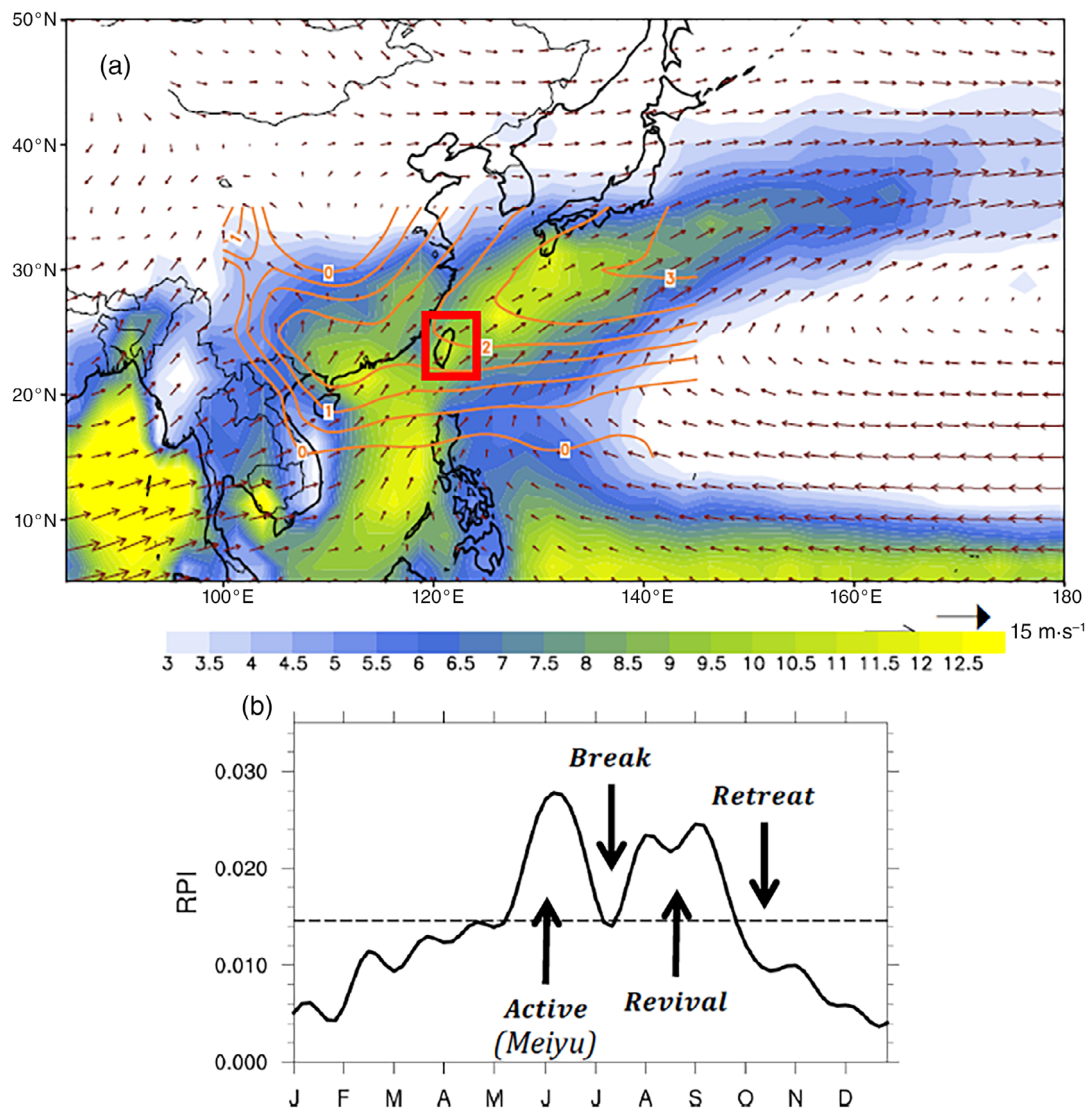


FIGURE 1 (a) Long-term mean 850 hPa wind vectors and Global Precipitation Climatology Project (GPCP) precipitation (shading) during the *Meiyu* peak season of May 20–June 10, overlaid with the 925 hPa meridional temperature gradient (yellow contour; only focused at the rain band). The data period is 1981–2000. Taiwan is indicated by the red box (21.25–26.25° N, 118.75–122.5° E). (b) Smoothed pentad (five day mean)-normalized precipitation during the year averaged in Taiwan of the red box in (a), indicated with the four phases of the East Asian summer monsoon (EASM) lifecycle

changes of the EASM rainfall have been investigated using global climate models (Kitoh *et al.*, 1997; Kitoh and Uchiyama, 2006; Li *et al.*, 2010; Inoue and Ueda, 2011; Kusunoki *et al.*, 2011; Seo *et al.*, 2013; Song *et al.*, 2014; He and Zhou, 2015; Zou and Zhou, 2015) and regional models (Zou and Zhou, 2016; Huang and Wang, 2017). Overall, anthropogenic warming is projected to change the EASM in two ways: general precipitation enhancement and a lengthening in the monsoon season. However, a recent study (Wu *et al.*, 2017) evaluating the simulations of spring precipitation in East Asia has found that lower resolution models exhibit a deficiency in capturing the vertical motion over the broad monsoon region. While most modelling studies focused on the entire duration of the EASM (June–August or May–September), few paid attention to the pronounced intra-seasonal and synoptic feature of the *Meiyu* rain band, which is also a challenge faced by global models.

The extent to which the observed change in *Meiyu* will continue in future requires further modelling diagnosis, and this motivates the present study. Following the observational analysis of Wang *et al.* (2016) and model investigation of the EASM by Wu *et al.* (2017), the present study assesses future changes of *Meiyu* precipitation and associated atmospheric features using Couple Model Intercomparison Project Phase 5 (CMIP5) model outputs. The paper is structured as follows. Section 2 provides data sources and the methodology. Section 3 presents the model evaluation and projection results. Section 4 discusses the simulations. Section 5 concludes.

2 | DATA SOURCES AND METHODS

For the observations, Climate Prediction Center Merged Analysis of Precipitation (CMAP) data (Xie and Arkin, 1997) and the Global Precipitation Climatology Project (GPCP) precipitation data (Adler *et al.*, 2003; Huffman *et al.*, 2009) were used at a five day mean frequency, provided by the NOAA Earth System Research Laboratory's Physical Sciences Division (PSD) (<https://www.esrl.noaa.gov/psd/>), both of which cover the period 1979–2016. The GPCP and CMAP data sets are both regarded as the observation and used interchangeably. For the climate projections, 17 models that provide daily variables form the Couple Model Intercomparison Project Phase 5 (CMIP5) (Taylor *et al.*, 2012) were used in the Historical and RCP8.5 experiments; for a description of these models, see Table 1. Following Knutti *et al.* (2010), only one model from each institute was selected, given that this sampling approach can avoid potential systematic bias when calculating multimodal ensemble mean trends.

The period 1981–2000 is used in the historical climate simulation; the period 2081–2100 is used in the future projection under the high-emission pathway or RCP8.5 as the time slice approach. Model resolutions were interpolated to a $2.5 \times 2.5^\circ$ grid; and daily time steps were averaged every five days to form the pentad means (for a discussion of model resolution, see Section 4).

Since each individual model has its unique bias in the amount of absolute rainfall, it is necessary to use model-dependent criteria to identify the simulated EASM onset, retreat and duration, instead of applying a fixed rainfall criterion as used in earlier observational analysis. Following Tung *et al.* (2014), the precipitation amount is converted into the ratio of a precipitation index (RPI), which is normalized by the amount that corresponds to the “height” or maximum of simulated precipitation in the cumulative distribution function (CDF), that is, where the simulated CDF height meets the observed CDF height of rainfall. Using the pentad-mean precipitation (73 time steps *per year*), the first 12 harmonic modes are then retained in order to focus on the predominant low-frequency variability that accompanies the EASM lifecycle (Chen *et al.*, 2004). In Tung *et al.*, the January mean precipitation was subtracted from each pentad and the difference was then normalized by its annual mean rainfall, obtaining a ratio that represents the RPI. For the depiction of *Meiyu* in Taiwan and the associated EASM phases, the areal average of nine CMAP/GPCP grids encompassing Taiwan (the red box in Figure 1a) were used to obtain the resultant RPI. This new variable of Taiwan RPI is shown in Figure 1b, where the onset is defined when the RPI first increases above the annual mean while the retreat is defined when the RPI decreases below it (Tung *et al.*, 2014).

3 | RESULTS

3.1 | Model evaluation and grouping

The precursor of *Meiyu* rainfall can be traced back to the onset of the Indochina monsoon rain band (Lin and Wang, 2002), the western Pacific monsoon (Murakami and Matsumoto, 1994; Chen *et al.*, 2004) and the Tibetan Plateau's heating impact on the westerlies (Chou *et al.*, 2011). Thus, by evaluating the simulation of Taiwan's precipitation lifecycle, one can obtain a credible indication about how well the models depict the dynamics driving the EASM. Using the onset day, retreat day and duration (between the onset and retreat days) as metrics, model precipitation is evaluated using the Taylor diagram (Taylor, 2001), which allows for the simultaneous examination of both temporal correlation and standard

TABLE 1 Model description, institute and its resolution

Model	Description, country and institute	Resolution
ACCESS1-0	Australian Community Climate and Earth System Simulator 1.0 Australia, CSIRO-BOM	192*145
bcc-csm1-1	Beijing Climate Center Climate System Model v.1.1 China, BCC	128*64(T42)
BNU-ESM	College of Global Change and Earth System Science, Beijing Normal University Earth System Model China, BNU	128*64(T42)
CanESM2	Canadian Earth System Model v.2 Canada, CCCma	128*64(T42)
CCSM4	NCAR Community Climate System Model v.4.0 USA, NCAR	288*192
CMCC-CM	Centro Euro-Mediterraneo sui Cambiamenti Climatici Climate Model Italy, CMCC	480*240
CNRM-CM5	Centre National de Recherches Meteorologiques (CNRM) Earth System Model v.5, France. CNRM-CERFACS	256*128(T85)
CSIRO-MK3-6-0	CSIRO Atmospheric Research, Mk3.6 Model Australia, CSIRO-QCCCE	192*96(T63)
FGOALS-g2	Flexible Global Ocean–Atmosphere–Land System Model, Grid-point v.2 China, LASG-CESS	128*60
GFDL-ESM2M	Geophysical Fluid Dynamics Laboratory Earth System Model Couple MOM4 Ocean Model USA, NOAA-GFDL	144*90
HadGEM2-CC	Met Office Hadley Centre, Hadley Global Environment Model 2—Carbon Cycle UK, MOHC	192*145
inmcm4	Institute for Numerical Mathematics, INMCM4.0 Model Russia, INM	180*120
IPSL-CM5A-MR	Institute Pierre-Simon Laplace with LMDZ4 Atmosphere Model with Medium Resolution France, IPSL	144*143
MIROC5	CCSR/NIES/FRCGC, MIROC Model V5 Japan, MIROC	256*128(T85)
MIROC-ESM-CHEM	CCSR/NIES/FRCGC, MIROC Earth System Model Japan, MIROC	128*64(T42)
MPI-ESM-LR	Max Planck Institute for Meteorology, Earth System Model—Low Resolution Grid Germany, MPI-M	192*96(T63)
MRI-CGCM3	Meteorological Research Institute, CGCM3 Japan, MRI	320*160(T106)
NorESM1-M	Norwegian Earth System Model 1—Medium Resolution Norway, NCC	144*96

deviation (*SD*). As shown in Figure 2, the correlations fall between 0.4 and 0.6 for the onset day (Figure 2a) and between 0.6 and 0.8 for the retreat day (Figure 2b), while the correlations for the monsoon duration are clustered between 0.4 and 0.7 (Figure 2c). Based on Tung *et al.* (2014) and Kitoh *et al.* (2013), these results are consistent with the CMIP5 models' overall performance in depicting the precipitation annual cycle within the EASM.

To account for precipitation variance, the Taylor Skill (TS) score introduced by Taylor (2001) is further derived in order to evaluate the model's performance with observation in a spatial distribution. One can then evaluate model (B) from observational (A) by combining the correlation co-efficient (*R*) and root mean square error (*E*) applied to A_t/B_t for the individual grid values and \bar{A}/\bar{B} for the area means:

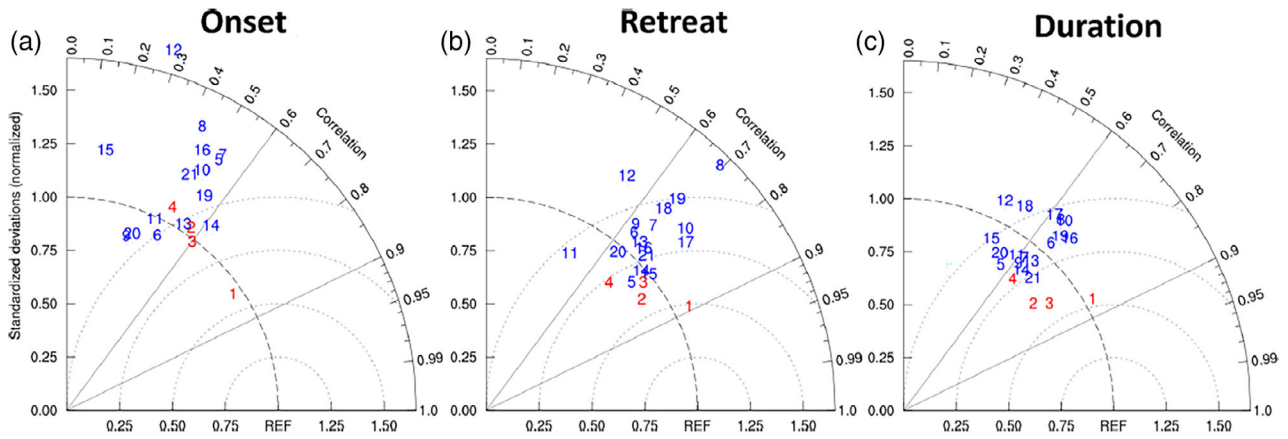


FIGURE 2 Taylor diagrams of the 17 models' performance compared with the observation (Climate Prediction Center Merged Analysis of Precipitation, CMAP) in the East Asian summer monsoon (EASM) (a) onset, (b) retreat and (c) duration dates over Taiwan. The identification numbers of models are consistent with Figure 2; red numbers emphasize the other observations (1: CMAP) and the three groups (2: ALL, 3: TOP-5 and 4: LAST-5). All models' correlation passed a 95% significant level, except the onset of inmc4

FIGURE 3 Taylor Skill (TS) scores of the 17 Couple Model Intercomparison Project Phase 5 (CMIP5) models plus the three groups (TOP-5, LAST-5 and ALL) and Climate Prediction Center Merged Analysis of Precipitation (CMAP), based on the East Asian summer monsoon (EASM) onset, retreat and duration dates. The red model identifications were the TOP-5 group; the blues represent the LAST-5. See the text for details

	Onset	Retreat	Duration
(1)CMAP	0.71	0.82	0.78
(2)ALLENS	0.39	0.70	0.61
(3)TOPSENS	0.43	0.65	0.68
(4)LASTSENS	0.30	0.52	0.45
(14)HadGEM2-CC	0.45	0.61	0.47
(21)NorESM1-M	0.29	0.57	0.53
(16)IPSL-CM5A-MR	0.27	0.55	0.54
(6)bcc-csm1-1	0.30	0.48	0.50
(19)MPI-ESM-LR	0.36	0.47	0.51
(5)ACCESS1-0	0.32	0.61	0.37
(7)BNU-ESM	0.32	0.50	0.45
(8)CanESM2	0.24	0.44	0.46
(10)CNRM-CM5	0.31	0.57	0.48
(13)GFDL-ESM2M	0.36	0.52	0.49
(15)inmc4	0.11	0.64	0.29
(17)MIROC5	0.21	0.61	0.43
(20)MRI-CGCM3	0.21	0.48	0.35
(9)CMCC-CM	0.20	0.46	0.44
(18)MIROC-ESM-CHEM	0.14	0.48	0.34
(12)FGOALS-g2	0.13	0.33	0.28
(11)CSIRO-Mk3-6-0	0.26	0.29	0.41

$$R = \frac{\frac{1}{n} \sum_{t=1}^n (A_t - \bar{A})(B_t - \bar{B})}{\sqrt{\frac{1}{n} \sum_{t=1}^n (A_t - \bar{A})^2 \times \frac{1}{n} \sum_{t=1}^n (B_t - \bar{B})^2}} \quad (1)$$

$$E = \sqrt{\frac{1}{n} \sum_{t=1}^n (A_t - B_t)^2} \quad (2)$$

$$T-S = \frac{4(1+R)^4}{(\hat{\sigma}_f + 1/\hat{\sigma}_f)^2(1+R_0)^4} \quad (3)$$

where $\hat{\sigma}_f$ is SD from the model to the observation; and R_0 is the maximum correlation attainable (or 1). Figure 3 classifies the skill of each model by colour coding them with 10 intervals between 0 and 1. The TS score is generally lower for the onset and relatively higher for the

duration and retreat. Based on the Taylor diagrams and TS score, two groups are selected with five models each for subsequent analyses: the top-ranking models (TOP-5) and the last-ranking models (LAST-5). The TOP-5 models are bcc-csm1-1, HadGEM2-CC, IPSL-CM5A-MR, MPI-ESM-LR and NorESM1-M, while the LAST-5 models consist of CMCC-CM, CSIRO-Mk3-6-0, FGOALS-g2, MIROC-ESM-CHEM and MRI-CGCM3 (Figure 3).

3.2 | Model diagnosis

The simulated pentad evolutions of historical precipitation are displayed in Figure 4b in conjunction with the observations (Figure 4a). The observed precipitation shows an increase in peak *Meiyu* rainfall and its reported delaying tendency, based upon the era comparison between 1979 and 1995 (solid line) and between 1996 and 2015 (dashed line). This is consistent with the finding of Wang *et al.* (2016). In terms of the historical climate (solid lines), TOP-5 models depict a clear *Meiyu* phase, and its timing of peak precipitation is consistent with observation (from early May to late June), even though the simulated *Meiyu* magnitude is not as large. The precipitation evolution is properly simulated with the discernible onset, break and revival phases, even though the retreat appears to be earlier than observed. This result is encouraging as it demonstrates TOP-5 models' capability at simulating the complex formation and migration mechanisms of the *Meiyu* rain band. The simulated break phase also implies a reasonable depiction of the western North Pacific subtropical high intrusion, which pushes the *Meiyu* rain band northward, causing a monsoon break in Taiwan (Chen *et al.*, 2004). In the LAST-5 models, precipitation within the *Meiyu* season is relatively weak compared with the TOP-5, and the revival phase is much broader. Both model groups underestimate spring precipitation in Taiwan between February and April, likely due to the important topographic effects of spring rainfall in Taiwan that cannot be simulated properly with coarse model resolution (Wu *et al.*, 2017). It is also possible that the reported sea surface temperature (SST) cold bias around Asia in the CMIP5 models can underestimate precipitation (Song and Zhou, 2014).

The RCP8.5 projections of precipitation in the TOP-5 and LAST-5 models are shown as dashed lines in Figure 4b–d. Both model groups produce a robust increase in *Meiyu* precipitation from the historical simulations with a slight delay in the timing of peak rainfall. In the TOP-5, the projected increase in *Meiyu* precipitation surpasses any precipitation change during the other seasons. Note that the revival phase appears to lengthen at both ends under global warming, a feature consistent

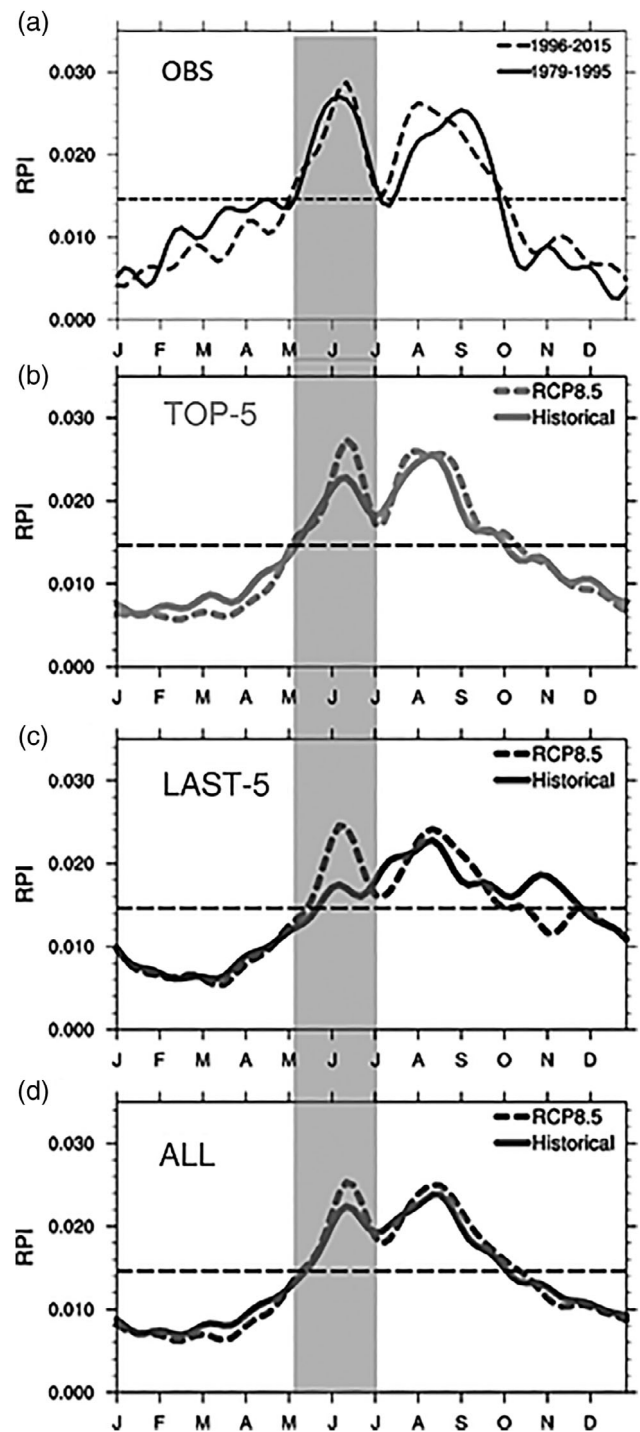


FIGURE 4 (a) Following Figure 1b for the observation (Global Precipitation Climatology Project, GPCP) precipitation annual distribution from 1979 to 1995 (dash lines) and from 1996 to 2015 (solid lines). (b) Represented TOP-5 (red), LAST-5 (golden) and observation in 1981–2000 (grey). Models simulate the annual cycle. (c–d) Simulated precipitation from the historical (solid lines) and RCP8.5 (dash lines) scenarios by the TOP-5, LAST-5 and ALL model ensembles, respectively. The period of *Meiyu* is highlighted by the grey band

with the earlier EASM studies projecting a lengthened monsoon (Kitoh and Uchiyama, 2006; Kusunoki *et al.*, 2011). In the LAST-5 models (Figure 4c), *Meiyu*

precipitation is increased even more (than the TOP-5), while the revival phase is delayed by about 10 days. To provide a larger ensemble viewpoint, Figure 4d shows the results from all 17 models. It still depicts an increase in *Meiyu* precipitation over Taiwan, suggesting that models unanimously project a stronger *Meiyu* in the warmer climate, regardless of their performance.

To depict the circulation changes associated with increased *Meiyu* precipitation, the horizontal distributions of 850 hPa winds and precipitation of the TOP-5 models are displayed in Figure 5, from the period May 20–June 10, for (a) historical climate, (b) future climate, (c) their difference and (d) that at 250 hPa. A visual comparison of Figure 5a with Figure 1a (observation) finds a marked resemblance, suggesting that the TOP-5 models simulate the low-level circulation and precipitation structure associated *Meiyu* quite well. This resemblance lends support to the present grouping of models, for the TOP-5 models indeed perform better in terms of the *Meiyu* rain band than does the LAST-5 (Figure 5e). In terms of the projected circulation change (Figure 5c), the TOP-5 depicts an elongated cyclonic anomaly extending from northern Taiwan to east of Japan, encircling the band-like rainfall increase between northeast Taiwan and southwest Japan. The precipitation increase appears to be moderate owing to the month-long period covered compared with the two week increase (Figure 4b). Nevertheless, this result echoes the finding of Ueda *et al.* (2015) that the subtropical western Pacific convection is projected to intensify when associated with an elongated cyclonic circulation enhanced by the strengthened inter-tropical convergence zone (ITCZ). Another notable feature is the increased precipitation in the deep Tropics, which reflects the reported intensification and northward migration of the ITCZ and the associated increase in EASM rainfall under a warmer climate (Kitoh *et al.*, 1997; Li *et al.*, 2010; Kusunoki *et al.*, 2011; Seo *et al.*, 2013; Song *et al.*, 2014).

In the LAST-5 models (Figure 5e–g), the historical *Meiyu* rain band appears weaker and displaced northward; this corresponds to a weaker monsoon trough in the South China Sea that acts to reduce the northward moisture transport. Interestingly, the future climate in the LAST-5 (Figure 5f) appears to be more similar to the observed one (than does its historical climate), while the rainfall increase over Taiwan in the LAST-5 (Figure 5g) is more pronounced than that in the TOP-5. The projected circulation change in the LAST-5 consists of an anticyclonic cell in the Philippine Sea, enhancing the low-level southwesterly flow over Taiwan, which contributes to *Meiyu* rainfall. This moist convergence can be further enhanced near Taiwan by the upper level trough anomaly (Figure 5h). Similarly, a well-defined, low-level

meridional temperature gradient also plays a critical role in affecting the strength of *Meiyu* frontal systems (Fu and Qian, 2011). Focusing on the summer, Seo *et al.* (2013) also found that the strengthening of the North Pacific subtropical high intensifies southwesterly winds towards coastal East Asia, which then increases moist convergence while enhancing precipitation.

Wang *et al.* (2016) showed that the observed intensification in *Meiyu* rainfall results from a southward migration of an unstable zone consisting of moisture transport and baroclinic forcing, which is driven by an upper level cyclonic anomaly over eastern China and a lower level anticyclonic anomaly in the subtropical Western Pacific. By examining the 250 hPa wind changes in Figure 5d,h, a prominent cyclonic circulation is observed over southwest China and the Himalayas in both groups. In the TOP-5, Taiwan is situated under the “jet entry”, while in the LAST-5, Taiwan is located beneath the “jet exit” (note that the wind patterns depicted here are anomalies, not the actual jet structure, but a similar synoptic analogy applies). The major difference between the two model groups lies in the fact that the TOP-5 produced a stronger westerly band stretching from east of Taiwan to east of Japan (Figure 5d), corresponding to the lower level cyclonic cell and the associated rain band (Figure 5c). In the LAST-5 (Figure 5h), Taiwan is situated under an upper level jet exit that is coupled with the lower level southwesterly winds (Figure 5g); this likely leads to the more enhanced precipitation than the TOP-5.

The implication of these anomalous wind fields is investigated by plotting the divergent circulation in Figure 6, in terms of the anomalous velocity potential (VP) and the divergent component of winds at 250 and 850 hPa. In the TOP-5 (Figure 6a, c), the change in the divergent circulations over Taiwan is not significant. In the LAST-5 (Figure 6d), a weak lower level convergence is discernible along the East Asia coastline (indicated by the curved VP contours), though a corresponding divergence is absent in the upper level (Figure 6b). These results suggest a large-scale circulation anomaly that would be unfavourable to precipitation enhancement, a finding that seems to contradict the increased *Meiyu* precipitation projected by both model groups. Given the lack of apparent dynamic causes for the projected *Meiyu* precipitation, it is plausible that thermodynamic processes play a more dominant role.

3.3 | Diagnosis of thermodynamics

As the lower tropospheric warming around Taiwan reaches approximately 4°C in the RCP8.5 simulations

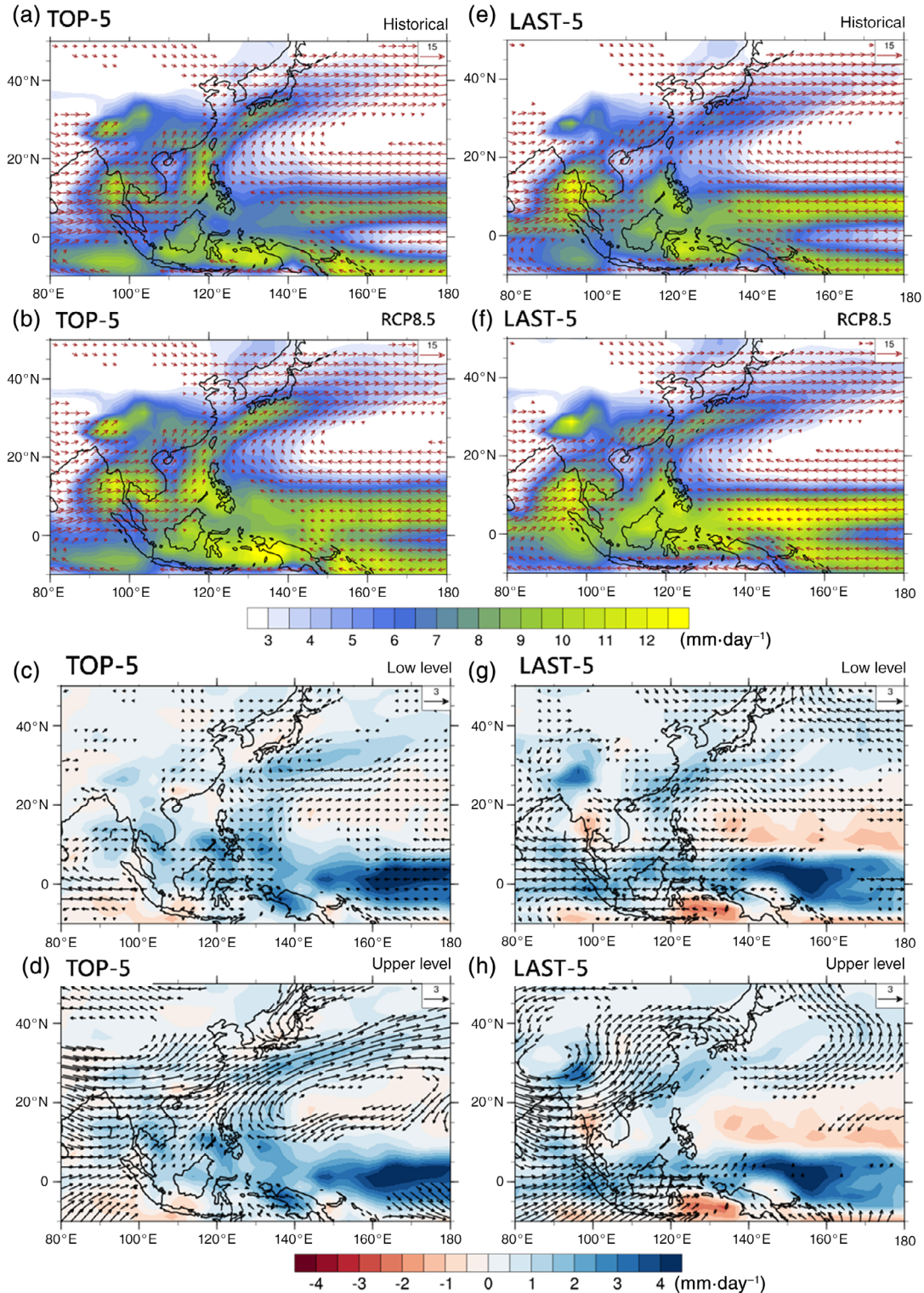


FIGURE 5 As for Figure 1a, but for the TOP-5 (a–d) and LAST-5 (e–h) ensembles of precipitation and 850 hPa wind vectors over the *Meiyu* period of May 20–June 10. Averages are shaded from (a, e) the present-day climate, (b, f) the RCP8.5 scenario, (c, g) their differences at 850 hPa, and (d, h) their differences at 250 hPa. The unit vectors of (a, b, e, f) are $15 \text{ m}\cdot\text{s}^{-1}$; those of (c, d, g, h) are $3 \text{ m}\cdot\text{s}^{-1}$, as shown in the top-right corner of each individual panel. Note that precipitation is the same at both levels

(data not shown), the moisture content in the atmosphere will rise much faster than the total precipitation amount, which will increase precipitation intensity while decreasing the duration or frequency of events

(Trenberth *et al.*, 2003). Thus, thermodynamics involving the Clausius–Clapeyron relation could be an important process from which the *Meiyu* precipitation intensity can strengthen; this factor can also be

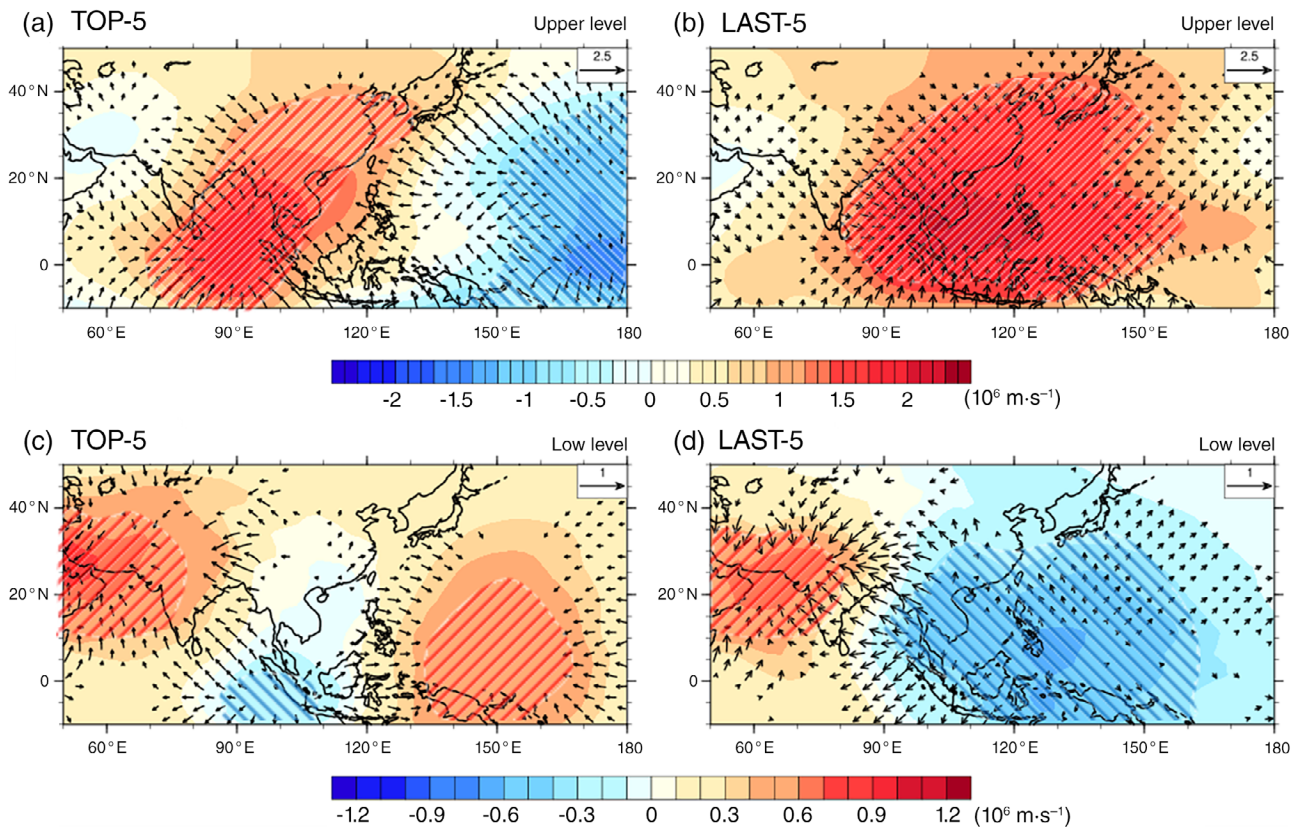


FIGURE 6 Differences in the 250 hPa velocity potential (VP) (shading) and divergent winds (wind vector) between RCP8.5 and the present-climate ensembles from the (a) TOP-5 and (b) LAST-5 model groups during the *Meiyu* period of May 20–June 10. (c, d) As for (a, b), but for the 850 hPa level. Only the divergent wind anomalies $> 2 \text{ m}\cdot\text{s}^{-1}$ for the upper level ($0.2 \text{ m}\cdot\text{s}^{-1}$ for the lower level) are plotted

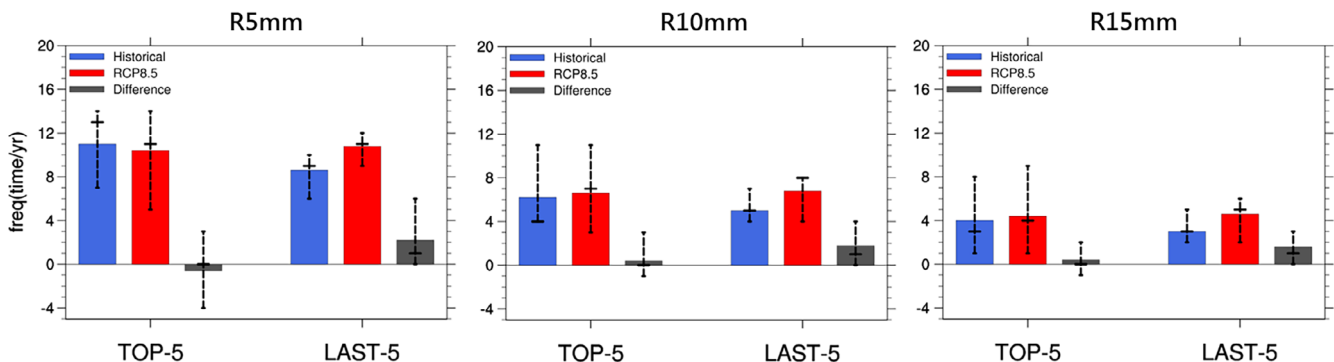


FIGURE 7 Frequency of daily precipitation events $> 5 \text{ mm}$ (R5mm), 10 mm (R10mm) and 15 mm (R15mm) over Taiwan ($21.25\text{--}26.25^\circ \text{ N}$, $118.75\text{--}122.5^\circ \text{ E}$) from May 15 to June 15, simulated from the TOP-5 (left) and LAST-5 (right) ensembles. Blue represents the present climate; red is for RCP8.5; and black is the difference. Error bars represent the TOP-5/LAST-5 groups models' distribution

compounded by the increased southwesterly low-level winds found in the LAST-5. To examine this possibility, we plot in Figure 7 the daily precipitation frequency change averaged from the nine grids around Taiwan. Three categories are created to depict daily precipitation events of > 5 , 10 and $15 \text{ mm}\cdot\text{day}^{-1}$ in all models. In the LAST-5, the projected increases in heavy-precipitation events are consistent across all three categories, ranging

from 25% to 45%. The higher increase in the LAST-5 may result from the increased southwesterly flow enhancing the moisture content in the air (*cf.* Figure 5g). In the TOP-5, only the frequency of stronger precipitation events reveals an increase, but for reasons unclear to the authors, it is milder than the LAST-5.

Figure 8 plots each year's pentad-mean 850 hPa relative humidity (RH) and precipitation averaged over

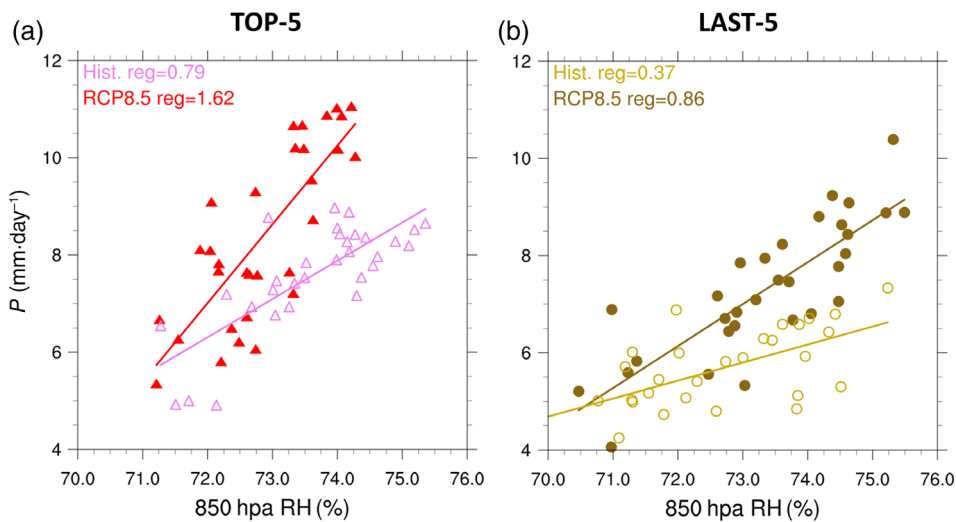


FIGURE 8 Scatter plot of daily precipitation ($\text{mm}\cdot\text{day}^{-1}$) and 850 hPa relative humidity (RH, %) in the *Meiyu* active period (May 20–June 10) represented in the (a) TOP5 and (b) LAST5 over Taiwan. The light/empty markers display historical data; the dark/filled are for RCP8.5

Taiwan during the *Meiyu* period for (a) TOP-5 and (b) LAST-5 to examine the effect of the Clausius–Clapeyron relation. The quasi-linear relationship between the two variables is apparent. There is a distinct and universal increase in the regression slope between historical and future climate scenarios, by 105% in the TOP-5 and by 132% in the LAST-5. The greater increase in the regression slope is found in the TOP-5 instead of the LAST-5 (Figure 8a, b). This result also suggests that RH in the TOP-5 will increase more than in the LAST-5 under the warmer climate, regardless of the low-level southwesterly increase. A similar finding was reported by Chen and Zhou (2015) concerning the regional SST change and associated impact on monsoon precipitation. It is arguable that a much warmer climate (by 4–5°C in East Asia under the RCP8.5; data not shown) can increase *Meiyu* precipitation even without consistent changes in the background circulation.

4 | DISCUSSION

Caution should be exercised when interpreting the presented model results. Even though most CMIP5 models simulate EASM annual precipitation well in terms of variance and amount (Kitoh *et al.*, 2013; Sperber *et al.*, 2013; Sperber and Annamalai, 2014), atmosphere–ocean general circulation models tend to require a high (20 km) resolution to simulate the *Meiyu* rain band properly (Kusunoki *et al.*, 2011). A companion study (Wu *et al.*, 2017) evaluated the simulations of pre-summer precipitation over the Maritime Continent and East Asia and found that lower resolution models exhibit a deficiency in capturing the vertical motion over the broad monsoon region. This systematic bias, caused largely by incorrect circulation–topography interaction, contributes to the lower performance in simulating the *Meiyu* rain band.

Furthermore, the documented uncertainty of the CMIP5 models in the projected changes of the western Pacific subtropical high can directly affect the simulation of the EASM rainfall (He *et al.*, 2015; 2017), and this aspect of simulation biases needs attention. Given these difficulties in simulating the mean *Meiyu* position, the extent to which the Intergovernmental Panel on Climate Change's (IPCC) models with a coarser resolution (> 100 km) depict the change of *Meiyu* remains uncertain and thereby requires further investigation.

The role of interdecadal variations in the EASM also needs to be considered when comparing historical change with projected change, especially in time-slice simulations. The early phase of the EASM has undergone a noticeable regime shift around the mid-1990s and its cause is manifold. For instance, Yim *et al.* (2014) found that the leading modes of the EASM variability have changed in association with a switch in the roles between the tropical Pacific and the North Atlantic, suggesting a large contribution of natural variability to decadal-scale climate change. Previous studies (e.g. Song and Zhou, 2015) have also noted the Pacific Decadal Oscillation's covariance with the East Asian monsoon rainfall. Paleoclimate studies (Liu *et al.*, 2014; 2015) also indicated recurrent multidecadal (20–40 year) changes in the EASM throughout the past millennium, implying that low-frequency variations may continue to be present in future. The existence of interdecadal variations in the EASM complicates the interpretation of any time-slice projections produced by climate models.

5 | CONCLUSIONS

The analysis presented herein follows the observational study of Wang *et al.* (2016) and the modelling study of Wu *et al.* (2017) to investigate the future changes of *Meiyu* in

Taiwan, using the Couple Model Intercomparison Project Phase 5 (CMIP5) outputs of the historical and future RCP8.5 simulations. Model evaluation was conducted based on the performance of the East Asian summer monsoon (EASM) lifecycle over Taiwan, resulting in two model groups: TOP-5 and LAST-5. While the TOP-5 models simulated the correct timing of the *Meiyu* precipitation increase in Taiwan, the LAST-5 models showed a weak *Meiyu* in the historical climate. However, both model groups projected a substantial increase in the *Meiyu* precipitation, despite their inconsistent projections of the circulation change. Putting it all together, a conclusion can be drawn that the observed increase in *Meiyu* precipitation in Taiwan is projected to continue under a rapidly warming climate, through the combined effects of (1) the Clausius–Clapeyron relationship which enhances intense precipitation as the Troposphere warms; and (2) the circulation anomalies that favour moisture pooling in Taiwan.

The analysis presented in the present paper can be applied to the general structure of the *Meiyu* rain band outside Taiwan (*cf.* Figure 5c, g), such as what was described for the July 2018 extreme *Meiyu/Baiu* rainfall in Japan (Wang *et al.*, 2019). The results presented herein and in Wang *et al.* (2019) also suggests that, even if the dynamic ingredients forming the *Meiyu* rain band will not change in the future, precipitation intensity can still increase due to the Clausius–Clapeyron relationship. This can then lead to more extreme rainfall during the *Meiyu* season. These model projections lend support to the observed trend in *Meiyu* rainfall, while providing a background of extreme *Meiyu* precipitation, as was witnessed in northern Taiwan in June 2017. Future work should focus on improving the sub-seasonal prediction of *Meiyu* precipitation and the associated extreme events to assist in disaster reduction and prevention.

ACKNOWLEDGEMENTS

Comments made by the reviewers are much appreciated. Y.-S.T. was supported by the Taiwan Climate Change Projection and Information Platform Project (TCCIP) programme (grant number MOST 107-2621-M865-001). S.Y.W. was supported by the US DOE-funded project HyperFACETS.

ORCID

Yu-Shiang Tung  <https://orcid.org/0000-0002-7191-8148>

REFERENCES

- Adler, R.F., Huffman, G.J., Chang, A., Ferraro, R., Xie, P.-P., Janowiak, J., Rudolf, B., Schneider, U., Curtis, S., Bolvin, D., Gruber, A., Susskind, J., Arkin, P. and Nelkin, E. (2003) The version-2 global precipitation climatology project (GPCP) monthly precipitation analysis (1979–present). *Journal of Hydrometeorology*, 4, 1147–1167. [https://doi.org/10.1175/1525-7541\(2003\)004<1147:TVGPCP>2.0.CO;2](https://doi.org/10.1175/1525-7541(2003)004<1147:TVGPCP>2.0.CO;2).
- Chen, T.-C., Wang, S.-Y., Huang, W.-R. and Yen, M.-C. (2004) Variation of the East Asian summer monsoon rainfall. *Journal of Climate*, 17, 744–762. [https://doi.org/10.1175/1520-0442\(2004\)017<0744:VOTEAS>2.0.CO;2](https://doi.org/10.1175/1520-0442(2004)017<0744:VOTEAS>2.0.CO;2).
- Chen, X. and Zhou, T. (2015) Distinct effects of global mean warming and regional sea surface warming pattern on projected uncertainty in the South Asian summer monsoon. *Geophysical Research Letters*, 42, 9433–9439. <https://doi.org/10.1002/2015GL066384>.
- Chou, M.-D., Wu, C.-H. and Kau, W.-S. (2011) Large-scale control of summer precipitation in Taiwan. *Journal of Climate*, 24, 5081–5093. <https://doi.org/10.1175/2011JCLI4057.1>.
- Fu, J. and Qian, W. (2011) The structure of a typical Mei-Yu front identified by the equivalent temperature. *Atmospheric and Oceanic Science Letters*, 4, 109–113.
- He, C., Wu, B., Zou, L. and Zhou, T. (2017) Responses of the summertime subtropical anticyclones to global warming. *Journal of Climate*, 30, 6465–6479. <https://doi.org/10.1175/JCLI-D-16-0529.1>.
- He, C. and Zhou, T. (2015) Responses of the western North Pacific subtropical high to global warming under RCP4.5 and RCP8.5 scenarios projected by 33 CMIP5 models: the dominance of tropical Indian Ocean–tropical western Pacific SST gradient. *Journal of Climate*, 28, 365–380. <https://doi.org/10.1175/JCLI-D-13-00494.1>.
- He, C., Zhou, T., Lin, A., Wu, B., Gu, D., Li, C. and Zheng, B. (2015) Enhanced or weakened Western North Pacific subtropical high under global warming? *Scientific Reports*, 5, 1–7. <https://doi.org/10.1038/srep16771>.
- Huang, W.-R. and Chen, K.-C. (2015) Trends in pre-summer frontal and diurnal rainfall activities during 1982–2012 over Taiwan and Southeast China: characteristics and possible causes. *International Journal of Climatology*, 35, 2608–2619. <https://doi.org/10.1002/joc.4159>.
- Huang, W.R. and Wang, S.Y.S. (2017) Future changes in propagating and non-propagating diurnal rainfall over East Asia. *Climate Dynamics*, 49, 375–389. <https://doi.org/10.1007/s00382-016-3348-4>.
- Huffman, G.J., Adler, R.F., Bolvin, D.T. and Gu, G. (2009) Improving the global precipitation record: GPCP version 2.1. *Geophysical Research Letters*, 36, L17808. <https://doi.org/10.1029/2009GL040000>.
- Inoue, T. and Ueda, H. (2011) Delay of the first transition of Asian summer monsoon under global warming condition. *SOLA*, 7, 81–84. <https://doi.org/10.2151/sola.2011-021>.
- Kitoh, A. and Uchiyama, T. (2006) Changes in onset and withdrawal of the East Asian summer rainy season by multi-model global warming experiments. *Journal of the Meteorological Society of Japan*, 84, 247–258. <https://doi.org/10.2151/jmsj.84.247>.
- Kitoh, A., Uchiyama, T., Endo, H., Krishna Kumar, K., aCavalcanti, I.F., Goswami, P. and Zhou, T. (2013) Monsoons in a changing world: a regional perspective in a global context. *Journal of Geophysical Research. Atmospheres*, 118, 3053–3065. <https://doi.org/10.1002/jgrd.50258>.
- Kitoh, A., Uchiyama, T., Yukimoto, S., Noda, A. and Motoi, T. (1997) Simulated changes in the Asian summer monsoon at times of increased atmospheric CO₂. *Journal of the*

- Meteorological Society of Japan. Series II*, 75, 1019–1031. https://doi.org/10.2151/jmsj1965.75.6_1019.
- Knutti, R., Furrer, R., Tebaldi, C., Cermak, J. and Meehl, G.A. (2010) Challenges in combining projections from multiple climate models. *Journal of Climate*, 23, 2739–2758. <https://doi.org/10.1175/2009JCLI3361.1>.
- Kusunoki, S., Mizuta, R. and Matsueda, M. (2011) Future changes in the East Asian rain band projected by global atmospheric models with 20-km and 60-km grid size. *Climate Dynamics*, 37, 2481–2493. <https://doi.org/10.1007/s00382-011-1000-x>.
- Li, J., Wu, Z., Jiang, Z. and He, J. (2010) Can global warming strengthen the East Asian summer monsoon? *Journal of Climate*, 23, 6696–6705. <https://doi.org/10.1175/2010JCLI3434.1>.
- Lin and Wang, B. (2002) The time–space structure of the Asian-Pacific summer monsoon: a fast annual cycle view. *Journal of Climate*, 15, 2001–2019. [https://doi.org/10.1175/1520-0442\(2002\)015<2001:TTSSOT>2.0.CO;2](https://doi.org/10.1175/1520-0442(2002)015<2001:TTSSOT>2.0.CO;2).
- Liu, J., Chen, J., Zhang, X., Li, Y., Rao, Z. and Chen, F. (2015) Holocene East Asian summer monsoon records in northern China and their inconsistency with Chinese stalagmite $\delta^{18}\text{O}$ records. *Earth-Science Reviews*, 148, 194–208. <https://doi.org/10.1016/j.earscirev.2015.06.004>. Available at: <http://www.sciencedirect.com/science/article/pii/S0012825215300064> [Accessed 20th January 2020].
- Liu, Z., Wen, X., Brady, E.C., Otto-Bliesner, B., Yu, G., Lu, H., Cheng, H., Wang, Y., Zheng, W., Ding, Y., Edwards, R.L., Cheng, J., Liu, W. and Yang, H. (2014) Chinese cave records and the East Asia summer monsoon. *Quaternary Science Reviews*, 83, 115–128. <https://doi.org/10.1016/j.quascirev.2013.10.021>. Available at: <http://www.sciencedirect.com/science/article/pii/S027379113004150> [Accessed 20th January 2020].
- Luo, X. and Zhang, Y. (2015) Interdecadal change in the seasonality of rainfall variation in South China. *Theoretical and Applied Climatology*, 119, 1–11. <https://doi.org/10.1007/s00704-013-1088-5>.
- Murakami, T. and Matsumoto, J. (1994) Summer monsoon over the Asian Continent and Western North Pacific. *Journal of the Meteorological Society of Japan. Series II*, 72, 719–745. https://doi.org/10.2151/jmsj1965.72.5_719.
- Sampe, T. and Xie, S.-P. (2010) Large-scale dynamics of the *Meiyu-Baiu* rainband: environmental forcing by the westerly jet. *Journal of Climate*, 23, 113–134. <https://doi.org/10.1175/2009JCLI3128.1>.
- Seo, K.-H., Ok, J., Son, J.-H. and Cha, D.-H. (2013) Assessing future changes in the East Asian summer monsoon using CMIP5 coupled models. *Journal of Climate*, 26, 7662–7675. <https://doi.org/10.1175/JCLI-D-12-00694.1>.
- Song, F. and Zhou, T. (2014) The climatology and interannual variability of east Asian summer monsoon in CMIP5 coupled models: does air–sea coupling improve the simulations? *Journal of Climate*, 27, 8761–8777. <https://doi.org/10.1175/JCLI-D-14-00396.1>.
- Song, F. and Zhou, T. (2015) The crucial role of internal variability in modulating the decadal variation of the East Asian summer monsoon–ENSO relationship during the twentieth century. *Journal of Climate*, 28, 7093–7107. <https://doi.org/10.1175/JCLI-D-14-00783.1>.
- Song, F., Zhou, T. and Qian, Y. (2014) Responses of East Asian summer monsoon to natural and anthropogenic forcings in the 17 latest CMIP5 models. *Geophysical Research Letters*, 41, 596–603. <https://doi.org/10.1002/2013GL058705>.
- Sperber, K.R. and Annamalai, H. (2014) The use of fractional accumulated precipitation for the evaluation of the annual cycle of monsoons. *Climate Dynamics*, 43, 3219–3244. <https://doi.org/10.1007/s00382-014-2099-3>.
- Sperber, K.R., Annamalai, H., Kang, I.S., Kitoh, A., Moise, A., Turner, A., Wang, B. and Zhou, T. (2013) The Asian summer monsoon: an intercomparison of CMIP5 vs. CMIP3 simulations of the late 20th century. *Climate Dynamics*, 41, 2711–2744.
- Takahashi, H.G. and Yasunari, T. (2006) A climatological monsoon break in rainfall over Indochina—a singularity in the seasonal march of the Asian summer monsoon. *Journal of Climate*, 19, 1545–1556. <https://doi.org/10.1175/JCLI3724.1>.
- Taylor, K.E. (2001) Summarizing multiple aspects of model performance in a single diagram. *Journal of Geophysical Research*, 106, 7183–7192.
- Taylor, K.E., Stouffer, R.J. and Meehl, G.A. (2012) An overview of CMIP5 and the experiment design. *Bulletin of the American Meteorological Society*, 93, 485–498. <https://doi.org/10.1175/BAMS-D-11-00094.1>.
- Trenberth, K.E., Dai, A., Rasmussen, R.M. and Parsons, D.B. (2003) The changing character of precipitation. *Bulletin of the American Meteorological Society*, 84, 1205–1217. <https://doi.org/10.1175/BAMS-84-9-1205>.
- Tung, Y.-S., Chen, C.-T. and Hsu, P.-C. (2014) Evolutions of Asian summer monsoon in the CMIP3 and CMIP5 models. *SOLA*, 10, 88–92. <https://doi.org/10.2151/sola.2014-018>. Available at: <http://jlc.jst.go.jp/DN/JST.JSTAGE/sola/2014-018?lang=en&from=CrossRef&type=abstract> [Accessed 20th January 2020].
- Ueda, H., Kamae, Y., Hayasaki, M., Kitoh, A. and Watanabe, S. (2015) Combined effects of recent Pacific cooling and Indian Ocean warming on the Asian monsoon. *Nature Communications*, 6, 1–8. <https://doi.org/10.1038/ncomms9854>.
- Wang, S.S.-Y., Kim, H., Coumou, D., Yoon, J.-H., Zhao, L. and Gillies, R.R. (2019) Consecutive extreme flooding and heat wave in Japan: are they becoming a norm? *Atmospheric Science Letters*, 20, e933. <https://doi.org/10.1002/asl.933>.
- Wang, S.-Y.S., Lin, Y.-H. and Wu, C.-H. (2016) Interdecadal change of the active-phase summer monsoon in East Asia (*Meiyu*) since 1979. *Atmospheric Science Letters*, 17, 128–134. <https://doi.org/10.1002/asl.603>.
- Wu, C.-H., Freychet, N., Chen, C.-A. and Hsu, H.-H. (2017) East Asian presummer precipitation in the CMIP5 at high versus low horizontal resolution. *International Journal of Climatology*, 37, 4158–4170. <https://doi.org/10.1002/joc.5055>.
- Xie, P. and Arkin, P.A. (1997) Global precipitation: a 17-year monthly analysis based on gauge observations, satellite estimates, and numerical model outputs. *Bulletin of the American Meteorological Society*, 78, 2539–2558. [https://doi.org/10.1175/1520-0477\(1997\)078<2539:GPAYMA>2.0.CO;2](https://doi.org/10.1175/1520-0477(1997)078<2539:GPAYMA>2.0.CO;2).
- Yim, S.-Y., Wang, B. and Kwon, M. (2014) Interdecadal change of the controlling mechanisms for East Asian early summer rainfall variation around the mid-1990s. *Climate Dynamics*, 42, 1325–1333. <https://doi.org/10.1007/s00382-013-1760-6>.
- Zou, L. and Zhou, T. (2015) Asian summer monsoon onset in simulations and CMIP5 projections using four Chinese climate

models. *Advances in Atmospheric Sciences*, 32, 794–806. <https://doi.org/10.1007/s00376-014-4053-z>.

Zou, L. and Zhou, T. (2016) Future summer precipitation changes over CORDEX-East Asia domain downscaled by a regional ocean–atmosphere coupled model: a comparison to the stand-alone RCM. *Journal of Geophysical Research. Atmospheres*, 121, 2691–2704. <https://doi.org/10.1002/2015JD024524>. Received.

How to cite this article: Tung Y-S, Wang S-YS, Chu J-L, *et al.* Projected increase of the East Asian summer monsoon (*Meiyu*) in Taiwan by climate models with variable performance. *Meteorol Appl.* 2020;27:e1886. <https://doi.org/10.1002/met.1886>